HHS Public Access

Author manuscript

Magn Reson Med. Author manuscript; available in PMC 2015 February 21.

Published in final edited form as:

Magn Reson Med. 2014 March ; 71(3): 1238–1250. doi:10.1002/mrm.24741.

Clinically viable magnetic poly(lactide-*co*-glycolide) (PLGA) particles for MRI-based cell tracking

Dorit Granot[a,$], **Michael K. Nkansah**[a,b,$], **Margaret F. Bennewitz**[a,b], **Kevin S. Tang**[a,b], **Eleni A. Markakis**[a,c], and **Erik M. Shapiro**[a,b,c,*]

[a]Molecular and Cellular MRI Laboratory, Magnetic Resonance Research Center, Department of Diagnostic Radiology, 300 Cedar Street, Yale University School of Medicine, New Haven, CT 06510, USA

[b]Department of Biomedical Engineering, Yale University, New Haven, CT 06511, USA

[c]Yale Stem Cell Center, Yale University School of Medicine, New Haven, CT 06520, USA

Abstract

Purpose—To design, fabricate, characterize and *in vivo* assay clinically viable magnetic particles for MRI-based cell tracking.

Methods—PLGA encapsulated magnetic nano- and microparticles were fabricated. Multiple biologically relevant experiments were performed to assess cell viability, cellular performance and stem cell differentiation. *In vivo* MRI experiments were performed to separately test cell transplantation and cell migration paradigms, as well as *in vivo* biodegradation.

Results—Highly magnetic nano- (~100 nm) and microparticles (~1–2 μm) were fabricated. Magnetic cell labeling in culture occurred rapidly achieving 3–50 pg Fe/cell at 3 hrs for different particles types, and >100 pg Fe/cell after 10 hours, without the requirement of a transfection agent, and with no effect on cell viability. The capability of magnetically labeled mesenchymal or neural stem cells to differentiate down multiple lineages, or for magnetically labeled immune cells to release cytokines following stimulation, was uncompromised. An *in vivo* biodegradation study revealed that NPs degraded ~80% over the course of 12 weeks. MRI detected as few as 10 magnetically labeled cells, transplanted into the brains of rats. Also, these particles enabled the *in vivo* monitoring of endogenous neural progenitor cell migration in rat brains over 2 weeks.

Conclusion—The robust MRI properties and benign safety profile of these particles make them promising candidates for clinical translation for MRI-based cell tracking.

Introduction

The field of MRI-based cell tracking has recently graduated from a research tool on animal models to clinical investigations with patients (1). The foundation behind MRI-based cell tracking is the use of superparamagnetic iron oxide particles for magnetic cell labeling.

*Corresponding author: Erik M. Shapiro, PhD, Department of Radiology, Michigan State University, 846 Service Rd, East Lansing, MI 48824, Tel: +1 (517) 884-3270; Fax: +1 (517) 432-2849, erik.shapiro@rad.msu.edu.

$These authors contributed equally

Using MRI experiments sensitive to local magnetic field inhomogeneities, i.e. T_2 and/or T_2^* mechanisms, these particles can be detected, generally as dark contrast (2, 3). Thus, by labeling cells with these particles, detection of the particles indirectly reports on the location of the cells. This principle has been used experimentally to monitor many cell transplant paradigms, from the migration of transplanted neural precursor cells in brain injuries (4), to hematopoietic and mesenchymal stem cells in myocardial infarct models (5), to immune cell trafficking (6).

Commonly used iron oxide nanoparticle formulations consist of either a 5 nm ultrasmall particle of iron oxide (USPIO) or 7 nm small particle of iron oxide (SPIO) crystal coated with dextran (7), bringing the total particle hydrodynamic size to 30 or 150 nm, respectively (8, 9). The 7 nm core/150 nm diameter SPIO, previously sold commercially as Feridex, was the most commonly used particle in the field and has been used for MRI-based cell tracking in humans (1). It must be emphasized that Feridex, while FDA approved for liver MRI, was not FDA approved for magnetic cell labeling. In most studies using iron oxide nanoparticles to visualize macrophage infiltration in humans, the iron oxide agent has been various non FDA-approved USPIOs, not Feridex (10).

An important characteristic of (U)SPIOs in general is that they are biodegradable within cells, with the iron entering the systemic iron pool of the individual (11). However, this advantage is overshadowed by numerous disadvantages as the particles relate to MRI-based cell tracking. First, USPIO and SPIO are less than 0.1% iron by volume. This results in extraneous space that could be filled with additional magnetic material. A second disadvantage is that (U)SPIOs require prior complexation with a transfection agent, either poly-l-lysine or protamine sulfate, in order to achieve sufficient cell labeling to enable *in vivo* detection (12–16). This introduces an additional experimental measure, potentially complicating clinical use. Third, a major disadvantage is that the FDA approved material, Feridex, is no longer being manufactured. While similar particle formulations continue to be sold by third parties, these products are not FDA approved.

Recently, a nanocomplex consisting of ferumoxytol with protamine sulfate and heparin (HPF) has been proposed as a clinically viable option for magnetic cell labeling (17). However, as with previous (U)SPIOs, prior complexation is required for iron oxide internalization and low intracellular iron concentration is achieved, ~ 0.75 – 2.5 pg Fe/cell, making sensitive detection of labeled cells challenging (17). Taken together, these three disadvantages strengthen the rationale to start over with a more robust magnetic cell labeling agent.

Inert micron sized iron oxide particles (MPIOs) have been introduced as an alternative to (U)SPIOs (2, 18). Many versions of these particles are available commercially. The construction of the beads incorporates multiple nanometer sized iron oxide cores within inert polymer matrices, thereby maintaining superparamagnetism. Some further incorporate high amounts of fluorescent dyes within the polymer matrix. Importantly, many of these MPIOs are >45% magnetite by weight. Thus, because of efficient packaging of iron into these particles, cells can be loaded with significantly more iron using MPIOs. Another major advantage of MPIOs is their higher r_2^* molar relaxivity, expressed as $s^{-1}mM^{-1}$, which

reflects the ability of a standard concentration of material to alter relaxation rates. The r_2* relaxivity is important because many cell tracking MRI experiments make use of gradient echo T_2*-weighted images. The r_2* relaxivities of Feridex and 0.76 micron MPIOs at 4.7T are 240 and 356 $s^{-1}mM^{-1}$ for SPIO and MPIO respectively, and at 11.7T, 498 and 851 $s^{-1}mM^{-1}$ respectively (18). The significance of these two advantages is that the ability to detect magnetically labeled cells is directly proportional to both the relaxivity of the agent as well as the iron content achieved by magnetic cell labeling. Indeed, robust single cell detection has been accomplished *in vivo* in animals using MPIOs (19–21).

Protocols have been developed for efficiently labeling various cell types with many different sized MPIOs (2). In most studies, cell labeling has been achieved by simple overnight incubation of particles in the cell culture medium, in a desired ratio for labeling, i.e. 40 particles per cell. Free particles can then be washed away from the dish, leaving behind labeled cells. Still, a major disadvantage of commercial MPIOs for magnetic cell labeling is that their polymer coatings are inert matrices. From a clinical perspective, it is generally favorable to have particles disintegrate following administration to limit long-term inflammation. Furthermore, for some applications, nanoparticles may simply label cells more efficiently than microparticles.

PLGA is an FDA-approved material and has been used for over thirty years for intracellular drug delivery (22–24). Importantly, PLGA degrades rapidly compared to other polymers, and its degradation products, lactic acid and glycolic acid, are well tolerated by the body (25). We have previously described the design, fabrication, and characterization of initial formulations of poly(D,L-lactide-*co*-glycolide) (PLGA)-encapsulated magnetite nanoparticles (NPs) and microparticles (MPs) (26). Conceptually, magnetic PLGA particles combine the advantages of Feridex and inert MPIOs into a single entity, that is, they are biodegradable and efficiently package iron. Initial formulations of magnetic PLGA particles were not yet optimized for magnetic content but preliminary viability and cell labeling studies were encouraging.

The work described in this manuscript builds upon this previous effort in several ways. First, particles were optimized for iron content both at the nanoparticle and microparticle size. Second, magnetic cell labeling was thoroughly investigated at multiple time points for several cell types. Third, a thorough in vivo biodegradation study was carried out. Fourth, these optimized PLGA-encapsulated iron oxide NPs and MPs were subject to a thorough pre-clinical evaluation in multiple stem and immune cell assays, including viability and physiology, stem cell differentiation, and immune cell cytokine release. Lastly, these particles were assessed for MRI-based cell tracking towards clinical and preclinical applications, using both a standard transplantation model and an innovative neural progenitor cell migration paradigm. Taken together, the present study represents the first ever complete evaluation of dedicated magnetic particles specifically designed for magnetic cell labeling for MRI-based cell tracking.

Methods

Fabrication and characterization of magnetic PLGA particles

Magnetic PLGA nanoparticles (NPs) and microparticles (MPs) were fabricated and characterized as described in Nkansah, et al (26). Weight ratios of magnetite to PLGA were 0:1, 1:1, and 2:1.

Magnetic cell labeling kinetics and physiological analysis

Magnetic PLGA NPs and MPs were assayed for cell labeling kinetics in culture. Mouse embryonic fibroblasts (STOs) were grown to near confluence (1×10^6 cells/well) in 6 well cell culture dishes in media, which consisted of Dulbecco's Modified Eagles Medium (DMEM) without L-glutamine supplemented with 10% fetal calf serum (FCS), 1% penicillin-streptomycin (PS), and 1% L-glutamine. Stock solutions of each NP and MP were diluted in media as described in Table 2. STOs were incubated in labeling media for 3, 6, 10, and 24 hours, after which cells were thoroughly washed to remove free particles and harvested. Iron content at each time point was assayed using inductively coupled plasma optical emission spectroscopy (ICP). Triplicate assays were performed.

Cell viability was determined by FACS analysis using Sytox Blue stain (Invitrogen) and validated by standard trypan blue protocol. Generation of reactive oxygen species (ROS) was measured with the general oxidative stress indicator CM-H2DCFDA (Invitrogen). Following 24 hour incubation with non-fluorescent version of the various particles, cells were extensively washed, collected in PBS at a concentration of $1 *10^6$ cells/mL and 10 μM of ROS reagent was added for 1 hour incubation at 37°C. Following removal of the loading buffer, cells were suspended in PBS and fluorescence was detected at 500nm. Experiments were run in quintuplicate (STOs) or triplicate (MSCs and macrophages).

Stem cell labeling and differentiation

Adult-derived rat hippocampal neural stem cells (Millipore Cat # SCR022, Billerica, MA) were cultured in growth media [N2 (Invitrogen, Carlsbad, CA)-supplemented Ham's DMEM/F12, 1% L-glutamine, 1% PS, and basic fibroblast growth factor (b-FGF, 20 ng/ml; Peprotech)] for 48 hours in chamber slides coated with human plasma fibronectin (Calbiochem, San Diego, CA). Cells were incubated for 24 hours with magnetic particles in media according to Dose 2 in Table 2, blank particles, or particle free media as unlabeled controls. After labeling, cells were washed with PBS and fed with differentiation media [FGF-deficient growth media plus 1% heat-inactivated FCS with retinoic acid (100 ng/ml, Stegment, Cambridge, MA)] for 1 week, then forskolin (5 μM, Stemgent, Cambridge, MA) for a second week.

For immunohistochemical analysis of labeled cells, NSCs were fixed in 4% paraformaldehyde for 10 minutes, washed twice with PBS, blocked and permeabilized with 2% normal donkey serum/0.3% Triton X-100 in KPBS for 1 hour at room temperature. Cells were then treated with primary antibodies [mouse anti-O4 IgM (Chemicon, Temecula, CA, 1:100), chicken anti-GFAP (Chemicon, 1:500), and mouse anti-type-III beta tubulin (TUJ1, Covance, Princeton, NJ, 1:500)] in 0.2M KPBS/0.3% Triton X-100 for 72 hours at 4°C,

washed, and incubated with suitable secondary antibodies [donkey anti-mouse IgM DyLight 549 for O4, donkey anti-chicken DyLight 649 for GFAP, and donkey anti-mouse IgG Rhodamine Red X for TUJ1; 1:250] in 0.2M KPBS/0.3% Triton X-100 for 1 hour at room temperature. Slides were coverslipped using ProLong® Gold Anti-Fade mount with DAPI and imaged using confocal microscopy (Leica TCS SP5 Spectral Confocal Microscope).

To enable flow cytometry of differentiation marker expression, NSCs labeled with the various particles and fed with differentiation media over a 2-week period were fixed with 4% paraformaldehyde for 20 minutes at room temperature washed with PBS and incubated for 45 mins in PBT-NDS (1x PBS, 3% BSA, 0.1% Triton-X-100, 10% normal donkey serum). NSCs were then incubated in primary antibodies on ice (using ratios described earlier) for 45 minutes in PBT (3% BSA/PBS for anti-O4), washed in 3% BSA/PBS and incubated in phycoerythrin (PE)-conjugated secondary antibodies (1:500; Jackson Immunoresearch, West Grove, PA) in PBT on ice for 30 minutes, washed in 3%BSA/PBS, and analyzed via flow cytometry. For the extracellular marker O4, NSCs were labeled in both fixed and live forms. O4-labeled live NSCs were also stained for viability using 7-aminoactinomycin D (7-AAD; BD Pharmingen, San Diego, CA). Expression levels were quantified using mean fluorescence intensities (MFI) of gated cell populations with fluorescence greater than secondary antibody-labeled control.

The ability of MSCs to differentiate down adipogenic and osteogenic lineages following labeling was investigated using previously published methods (27).

Immune cell labeling and cytokine release

Macrophages were labeled with magnetic PLGA particles and were assayed for cytokine release. Bone marrow cells were harvested from Sprague Dawley male rat femurs and cultured in RPMI containing 10% FCS, 1% PS, 1% L-glutamine, and 20 ng/ml macrophage colony stimulating factor at 37°C in a 5% CO_2 incubator for 7 days to allow them to differentiate into macrophages (28). Macrophages were labeled for 24 hours with magnetic particles in media according to Dose 2 in Table 2, blank particles, or particle free media as unlabeled controls, after which TNF-alpha and IL-6 ELISAs (Thermo Scientific, Logan UT) were performed on the supernatant to test for immunological activation of the macrophages by the particles. Stimulation of macrophages was initiated by addition of 2 μg/ml lipopolysaccharide for three hours. Controls were unlabeled macrophages. Experiments were run in triplicate.

In vivo MRI

Animal experiments were approved by the Yale Animal Care and Use Committee.

In vivo biodegradation—*In vivo* biodegradation of PLGA NPs was investigated using a procedure originally designed by Saebo, et al (29–31). PLGA 2:1 NPs was prepared at 1 mg Fe/ml in 0.9% saline and injected via tail vein into 8 week old CD-1 female mice at a dose of 2 mg Fe/kg (n=5). Mice were on average 30 g, and so received 60 μl injections. Mice underwent serial MRI for 12 weeks (time points were 1 day, 2 weeks, 4 weeks, 7 weeks, 9 weeks and 12 weeks post injection), after which they were sacrificed. Sacrifice was carried

out by intracardiac perfusion of saline. MPIOs and Feridex were similarly prepared and injected into mice (n=5 for each) and were scanned serially for all 12 weeks, after which they were sacrificed. A set of control animals receiving no injections was also scanned (n=5). The MRI procedure consisted of a respiratory gated, multislice T_2* mapping protocol, acquired on a 4.0T Bruker Biospec. A separate transmit volume and surface receive coil were used to enhance sensitivity and restrict the field of view to the liver. Mice were anesthetized with 1% isoflurane delivered via nosecone in 100% oxygen. Image resolution was 200 × 200 microns; 8 TE were acquired, spaced 3 ms apart. Particle remnant was calculated as fractional R_2* relative to R_2* of liver at Day 0. Data were also baseline corrected for the increase in R_2* of normal mouse liver over the course of the twelve week long experiment.

MRI of cell transplantation—MSCs were labeled in culture with 1:1 NPs for 10 hours after which uninternalized particles were removed by washing. Rats were anesthetized with 3% isoflurane in 90% oxygen/10% medical air, orally intubated, and mechanically ventilated at 65 breaths/minute. Respiratory patterns and end tidal CO_2 were monitored. MSCs were stereotactically injected into the rat cortex at three doses; 10, 100 and 1000 cells, all in 5 μl. A fourth injection was an injection of 1000 unlabeled cells. MRI was then immediately performed on an 11.7T Varian system, VnmrJ 2.3 software. Separate transmit-only volume (70 mm birdcage coil) and receive-only surface coils (35 mm diameter ring) were used. T_2* weighted 3D gradient echo MRI was performed using the following imaging parameters: FOV 2.56 cm^3, matrix 256^3 or 128^3 (100 μm or 200 μm isotropic voxel size, respectively), TR = 30 ms, TE = 8 ms.

MRI of endogenous neural progenitor cell migration—MRI-based cell tracking was tested using our well-developed paradigm of *in vivo* labeling and tracking of endogenous rat neural progenitor cells (32). Under anesthetic conditions as stated above, 20 μL of PLGA 1:1 MP (10 mg/mL) were stereotactically injected into the right anterior lateral ventricles of adult Sprague-Dawley rats at 1.5 mm caudal, 1.5 mm medial lateral from bregma, 3 mm into the brain (n=6, 180–200 g; Harlan, Indianapolis, Indiana) (32). One animal was similarly injected with 20 μL of 1.63 micron MPIO (10 mg/mL).

MRI was performed as described above using the following imaging parameters: FOV 2.56 cm^3, matrix 256^3 (100 μm isotropic voxel size), TR = 30 ms, TE = 8 ms. Following MRI, animals were revived and returned to the animal facility. Subsequent MRI scans were performed on days 1, 7, and 14 post injection.

CNR calculations, which determine the quality of the particles and labeling, and volume fraction of contrast in the OB, which measures the rate of endogenous progenitor cell migration, were performed for the PLGA MP and compared to inert MPIO cohorts as previously described (33).

At the end of the MRI sessions, rats were transcardially perfused with 0.1 M PBS, followed by 4% paraformaldehyde pH 9.5. Brains with intact olfactory bulbs were excised and processed for frozen sections by post-fixing in 4% paraformaldehyde with 10% sucrose for three days at 4°C. Brains were then embedded in TissueTek® embedding compound, and

frozen. Sagittal sections (16 μm) were cut on a cryostat, and standard Prussian Blue staining with nuclear fast red counterstaining was performed to identify iron in the brain.

Statistical evaluation

Statistical analysis for the significance of differences in particle sizes, differences between labeling time points, and change in CNRs and volume fractions was performed using the Student's t-test (2 tails, unpaired). For cytokine release experiments, Student's t-tests (2 tails, unpaired) were performed on individual particle formulations versus unlabeled cells and only within stimulated or unstimulated subsets. For analyzing stem cell differentiation data, one-way ANOVA was used to analyze differences between groups with a post ad hoc Tukey test to evaluate significance ($p<0.05$ was considered statistically significant).

Results

Characterization of magnetic PLGA particles

Magnetite was synthesized by thermal decomposition of iron oleate, achieving uniform 8–10 nm single domain crystals (34). Then, fluorescent, magnetic PLGA NPs and MPs were fabricated employing oil in water emulsion methodologies, using three different magnetite:PLGA weight ratios; 0:1, 1:1and 2:1 (26). By scanning electron microscopy (SEM), NPs and MPs had average diameters of 95–105 nm and 0.9–2.1 μm, respectively (Figure 1), with low polydispersity, especially for the NP preparations. Particles attempted with magnetite:PLGA weight ratios higher than 2:1 did not form NPs or MPs (data not shown). Table 1 lists the particle sizes and iron content for the different groups of particles made. Particles fabricated with higher concentrations of magnetite showed no difference in spherical morphology or gross surface characteristics from those made using a lesser amount. Increasing the magnetite:PLGA weight ratio to 2:1 was successful in augmenting the magnetite content in the MPs from 58.2% to theoretical limits of 66.1%, while achieving even higher than theoretical limits of magnetite weight percent for NPs, up to 83.7%. This is likely due to ultrasound-induced degradation of polymer during fabrication at high magnetite:PLGA weight ratios and is consistent with previous observations (35),(36). Magnetite volume fractions of particles (26.4, 33.4, 25.2, 57.0 vol% for MP 1:1, 2:1 and NP 1:1, 2:1 respectively) were at least twice that of Bangs beads (13 vol%), and compared favorably with the random close packing limit of 63.4 vol% for monodisperse spheres in a unit-volume.

Measured r_2 and r_2* molar relaxivities for both magnetic MPs formulations were consistent with static dephasing regime relaxation theory, with low r_2 (44.7, 38.7 $s^{-1}mM^{-1}$ iron, 1:1, 2:1 MP respectively) and high r_2* (384.1, 614.1 $s^{-1}mM^{-1}$ iron, 1:1, 2:1 MP respectively) (37). Relaxivity for NP suggest a transition from diffusion regime to static dephasing regime for 1:1 NP to 2:1 NP as 1:1 NP had high r_2 and r_2* (196.0, 659.1 $s^{-1}mM^{-1}$ iron, respectively) while 2:1 NP had low r_2 and high r_2* (28.5, 243 $s^{-1}mM^{-1}$ iron, respectively) (37). For comparison, we have previously measured r_2 and r_2* relaxivities for Feridex on the same MRI system to be 110.5 and 214.8, respectively (26). Converting these relaxivity values to per particle numbers reveals that NP are 360–820 times more efficient than

Feridex for r_2 relaxivity and 1400–1600 times better for r_2* relaxivity. MP relaxivity on a per particle basis are equivalent to inert MPIOs.

Magnetic cell labeling and cytotoxicity of PLGA particles

The kinetics of magnetic cell labeling with the different particle formulations was determined in mouse embryonic fibroblasts. Stock solutions of each NP and MP were prepared as outlined in Table 2. Quantification of iron content within the cells by ICP analysis revealed two findings. First, all particle types labeled cells in a time-dependent manner. In the case of 2:1 MPs, maximal labeling occurred at 6 hours for the two lowest doses and at 10 hours for the highest dose (Figure 2a). It should be noted that for all particle types, substantial cell labeling occurred at 3 hours, particularly for NP 2:1 and the two MP particle types. This is potentially important for some primary cell types, such as hepatocytes, which undergo rapid phenotypic changes in cell culture. A second finding was that when exposed to a common dosing paradigm where NPs and MPs were added at equal particle numbers within groups (Dose 2, Table 2), as expected, cells that were labeled with particles containing higher magnetite content, 2:1 NPs and 2:1 MPs (83.7% and 66.1% magnetite respectively) were found to contain significantly more iron per cell than same size particles containing less iron (Figure 2b). Cell labeling occurred in strict dose dependent fashion for MPs (Figure 2a), while for NPs the relationship between magnetic cell labeling and dose was less clear. Indeed, PLGA NPs can exhibit aggregation, especially in high concentration. To alleviate this and facilitate NP resuspension following freeze drying, cryoprotection during particle fabrication will likely be necessary in the any final clinical particle formulation (38, 39). Dose dependent cell labeling data for all four magnetic particle types are shown in Supplementary Figure 1.

Internalized magnetic particles can be diluted during cell division and this needs to be taken into account when designing cell transplantation experiments with different cell types. As expected, iron retention within slowly dividing mesenchymal stem cells was substantially preserved over 8 days (Fig. 3a). On the other hand, iron in fast dividing cells was essentially lost after eight days (Fig. 3b), consistent with recent findings using HPF in fast dividing cells (17).

Initial attempts to label T-lymphocytes in suspension by simple incubation proved unsuccessful, likely due to settling of the heavy magnetic particles to the bottom of the dish. Indeed, T-lymphocyte labeling with any magnetic particle that does not use a transfection agent or antibody-mediated chemistry is extremely challenging. For example, overnight labeling of T-lymphocytes in culture with HPF (which includes protamine sulfate) is only able to achieve 0.75 pg Fe/cell(17).

The effect of internalized particles on cell viability and generation of reactive oxygen species (ROS) was evaluated. Cell viability for slow dividing cells (rat mesenchymal stem cells MSCs) and fast dividing cells (STO mouse embryonic fibroblasts) from 1 to 8 days post labeling was found to be largely unaffected by the label (Figure 3c,d). For one sample, MSCs labeled with MP 0:1, a non-magnetic particle, a statistically significant ($p=0.03$) loss of viability was observed one day following labeling, that was not observed at the 8 day time point. In macrophages, generation of ROS 1 day following labeling was insignificant

between labeled and unlabeled cells (Figure 3e). ROS generation for labeled STOs 1 day following labeling showed significant changes only for MP 0:1 and NP 2:1 samples. 5 days post labeling, significant differences in ROS production were found in all samples except MP 2:1 as compared to unlabeled cells (Figure 3f). These experiments were performed on cells that were labeled for 24 hours using unsterilized research grade particles, reaching iron contents that in some cases, based on Figures 2 and Supplementary Figure 1 could be higher than 50 pg/cell. While these results do suggest a potential mild negative effect of the particles on cellular health, definitive information on cellular harm should be obtained from experiments using sterile, optimally formulated, clinical grade material with varying internalized iron content.

Stem cell differentiation and immune cell cytokine release

We evaluated two different rat stem cell types, rat hippocampal neural stem cells (NSCs) and rat MSCs, for multilineage differentiation capacity following magnetic cell labeling. Multipotent NSCs generated cells of all three neural lineages as confirmed by immunocytochemistry for oligodendrocytes (using the antibody to O4, a sulfatide on pro-oligodendrocytes, and type-1 and type-11 oligodendrocytes) (40), astrocytes (using the antibody to glial-fibrillary acidic protein, GFAP) (41) and immature neurons (using the antibody to type III beta tubulin, Tuj1) (42) (Figure 4a). Furthermore, using both immunocytochemical and flow cytometry experiments, the proportions of differentiated cell types generated from magnetically labeled NSCs showed no statistically significant differences when compared to unlabeled differentiated NSCs (Figure 4b).

Supplementary Figure 2 shows MSCs labeled with all four particle types prior to differentiation. Labeling MSCs with NPs/MPs did not affect their ability to differentiate into fat and bone cells, compared with unlabeled controls, (Figure 5). Furthermore, the number of adipocytes generated from magnetically labeled MSCs was not statistically different from the number of adipocytes generated from unlabeled MSCs.

Primary bone-marrow derived macrophages were labeled for 24 hours with particle concentrations detailed as Dose 2 in Table 2, and were assayed for their ability to secrete inflammatory cytokines following stimulation by LPS (43). For all particle types, cytokine secretion by labeled cells following stimulation was uninhibited, while importantly, the presence of the particles themselves caused only minimal, albeit statistically significant, stimulation of cytokine release (Supplementary Figure 3). This minimal stimulation is commonly observed for immune cells following labeling with a variety of nanomaterial types (reviewed in (44)).

In vivo biodegradation

The *in vivo* biodegradation of NPs was investigated using a procedure initially designed by Briley-Saebo, et al (29–31). Serial MRI of the liver over 12 weeks was used to investigate the biodegradation of the three particle types (Figure 6). As expected, Feridex was rapidly degraded and the iron recycled within two weeks. Also as expected, inert MPIOs exhibited no biodegradation. 2:1 NPs exhibited an intermediate biodegradation rate, with 80% clearance of the iron at the end of 12 weeks.

In vivo MRI-based cell tracking

Two MRI-based cell tracking experiments were performed. The first was a standard cell transplant paradigm. Rat MSCs cells were labeled in culture with 1:1 NPs for 10 hours using Dose 2 and injected into a rat brain at three doses; 10, 100 and 1000 cells. A fourth injection was an injection of 1000 unlabeled cells. 3D gradient echo MRI revealed robust detection of the 10-cell injection at 100 microns resolution, while 100 cells were detected at 200 microns resolution (Figure 7). This second low resolution study was performed as a basis for more likely achievable clinical image resolution (45).

MRI-based cell tracking was tested using our well developed paradigm of *in vivo* labeling and tracking of endogenous rat neural progenitor cells (32, 33) comparing 1:1 MPs and inert MPIOs. The *in vivo* potential of PLGA MPs was assessed via two parameters. The first is the contrast to noise ratio (CNR) calculation, which determines the quality of the particles. The second parameter is the volume fraction of contrast in the OB, which determines applicability of these particles in an established model of endogenous progenitor cell labeling and tracking. As can be seen in Figure 8a, dark contrast on T_2* weighted MRI was detected from the lateral ventricle along the rostral migratory stream to the olfactory bulbs, as early as 1 day post injection, in concomitance with results obtained using inert MPIOs (Figure 8b) (33). This contrast then moved into the OB at day 7, with little increase at day 14. Figure 8b shows the data from one animal injected with inert MPIOs and reveals an identical time course. CNR measurements of the dark contrast regions (Figure 8c) revealed no statistically relevant differences in dark contrast hypointensity during the two-week MRI-based cell tracking paradigm, in line with the slow biodegradation of the NPs. There was, however, significantly greater CNR achieved with PLGA MPs than with inert MPIOs at all time points. Quantification of the volume of dark contrast in the OB from both cohorts of animals (Figure 8d), indicative of the migration time course of neural progenitor cells, matches the known migration time course from purely histological studies (46) as well as from previous MRI studies employing inert MPIOs as the contrast agent (33). However, while the time course is identical between the PLGA MPs and inert MPIOs, PLGA MPs have nearly four-fold higher volume content than inert MPIOs at days 7 and 14. This could be due to either higher labeling efficiency (# of cells initially labeled) or stronger contrast in labeled cells (more particles in cells). Prussian blue staining of histological sections from animals injected with PLGA MPs revealed the presence of iron within this migratory pathway (Figure 8e), indicating that indeed magnetic PLGA MPs can enable the same type of advanced MRI-based cell tracking paradigms that inert MPIOs enable (33) and potentially with better imaging characteristics.

Discussion

A critical component of MRI-based cell tracking is robust magnetic particles for cell labeling. Dextran coated (U)SPIO nanoparticles have played a major role in progressing the field from animal research to initial human evaluation. While this acceleration has been exciting, the MRI particles used to perform these studies are non-ideal and an FDA approved version is no longer commercially available. This presents a critical barrier to

progress in the field. Thus, there exists a need to formulate new, robust agents with the possibility for FDA approval.

In this work, we describe the preparation and pre-clinical evaluation of clinically viable magnetic polymer nano- and microparticles. Particles rapidly labeled cells safely, to high intracellular iron levels, without affecting the ability of stem cells to differentiate properly or for immune cells to perform vital inflammatory functions. These particles were also proven useful for MRI-based cell tracking in two *in vivo* animal models.

Moving forward, next generation particles for magnetic cell labeling in a clinical setting should possess four properties. First, they should have high iron content. For a number of reasons including magnetic field strength, the use of anesthetized animals, and the size of the MRI coils used, small animal MRI is capable of achieving very high image resolution, upwards of 50 microns, *in vivo*. As such, it is possible to detect low numbers of magnetically labeled cells labeled either with particles which deliver iron efficiently, i.e. MPIO (19–21), or with particles deficient of iron, i.e. (U)SPIO (47). However, as we transition to MRI-based cell tracking in humans, where image voxel sizes necessarily increase (image resolution decreases) (45), detection of the same low number of cells as the animal experiments will require magnetic particles that efficiently deliver iron. This will be most critical in detecting small numbers of cells in either migration/homing type procedures or for diagnostic purposes. The particles we fabricated in this work were optimized to contain high iron content, minimally 57% weight, ranging as high as 84%, and exceptionally high r_2* relaxivity, and have the potential to enable exceptionally highly sensitive cell detection, even in humans. Directly comparing NPs to Feridex reveals that NPs are 2–3 orders of magnitude better for magnetic cell labeling and deliver ten times more iron to cells than ferumoxytol/heparin/protamine sulfate complexes (HPF) (17). Indeed, MRI was capable of robustly detecting 10 transplanted cells in rat brain at 100 micron isotropic resolution, commonly performed in animals, and 100 cells at 200 micron resolution, a more realistic image resolution using high field human MRI. This is at least ten times more sensitive than recent reports using HPF labeled cells, where 1000 cells represented a minimal detection capability (17).

A second property is that particles should not interfere with cellular processes. In this work, we have shown that the presence of internalized magnetic particles were non-interfering in the ability of stem cells to differentiate properly or for immune cells to perform vital inflammatory functions. This has been a common finding among many magnetic particle formulations. Furthermore, magnetically labeled cells were capable of cytokine release following stimulation. Interestingly, there was low but significant cytokine release simply from magnetic cell labeling itself. This phenomenon is worth investigating using pharmaceutical grade particles produced in a sterile, GMP environment, which would be the next logical step for clinical translation. Indeed, the particles used in these studies were not sterilized. Lastly, the innocuousness of the particles was corroborated in the *in vivo* MRI experiment, where the presence of internalized MPs did not interfere with the rate of labeled neural progenitor cell migration in the brain.

Thirdly, particles should be easy to manipulate for cell labeling, both for maintaining control over final cell labeling potential, as well as ease of use. Indeed, it may be important to maintain control over final cell labeling potential, as it has been demonstrated that cells can be over-labeled and hence, affect critical cellular properties (48, 49). The necessity for mixing particles with transfection agents prior to magnetic cell labeling (12) or the requirement of using serum free media for a few hours then supplementing with serum containing media (17) opens up experimental avenues either for errors or for additional requirements for optimization for particular cell types. Ideally, particles should be ready to use for magnetic cell labeling right out of the bottle. Multiple studies have demonstrated that magnetic cell labeling using (U)SPIO only occurs when combined with the use of transfection agents (13, 14, 16, 50) or, in some instances, the use of electroporation/ sonoporation techniques (51, 52). In this work, sufficient magnetic cell labeling was accomplished at 3 hours using both NPs and MPs, simply by incubating particles with cells in culture. Most importantly, PLGA NPs show high labeling efficiency without the use of a transfection agent. A multitude of factors could explain these results. Key among these is that the magnetic PLGA NPs are heavier than (U)SPIO and sink easily in the labeling media, rapidly contacting plated cells.

Lastly, particles should be biodegradable, with known degradation profiles and safe degradation byproducts. Magnetic PLGA particles have two different degradation phenomena; degradation of the polymer encapsulant and dissolution of the iron oxide cores. Previous work on investigating these two processes in lysosomal mimicking media demonstrated that magnetic PLGA particles exhibit rapid degradation of the polymer coating during the first two weeks, followed by slower degradation over the next 4 weeks (26). Iron dissolution was slower but complete at 100 days. Our *in vivo* biodegradation study revealed that NPs degraded ~80% over the course of 12 weeks, or 84 days, matching closely the *in vitro* degradation characteristics. Whether this degradation time proves to be too slow still needs to be determined and small modifications to the fabrication scheme and materials will allow for faster degradation, such as the use of smaller iron oxide nanocrystals or using alternative PLGA compositions. The measured CNR of the MRI data demonstrated that even within these degradation windows, uniformly sustained MRI contrast could be generated for several weeks.

We chose to fabricate MPs as well as NPs. Indeed, while most work in magnetic cell labeling has historically concentrated on the use of NPs for cell labeling (53), magnetic MPs have proven useful in a number of MRI-based cell tracking paradigms (54). A benefit of MPs over NPs is that, in principle, only single MPs will be necessary for robust detection by MRI at high resolution (3). This has implications in using MRI to monitor transplantation of cells which are challenging to label, such as demonstrated in the work here with endogenous neural progenitor cells, or which are expected to divide multiple times, thereby diluting the label (55). Furthermore, due to clustering of such a significant amount of iron oxide within a single entity (56), MPs exhibit an increased r_2* molar relaxivity versus NPs, even for similar iron weight percents. Thus, if one is using gradient echo MRI methodologies, which are most sensitive to r_2*, magnetic MPs are more sensitive than NPs. However, for some cell

labeling paradigms or certain cell types, magnetic cell labeling with NPs may simply be easier than MPs.

The clinical utility of PLGA encapsulated magnetite MPs and NPs will require two key determinations. The first is their potential for enhanced clinical management or unique capabilities, especially when compared to more mature particle platforms. Indeed, it is acknowledged that dextran coated iron oxide particles such as Feridex, and ferumoxytol have been through rigorous FDA approval processes and have been optimally formulated for shelf life and intravenous delivery. But with respect to magnetic cell labeling for MRI-based cell tracking, there exist significant limitations for their use. Specifically, the weak magnetic properties of these particles and the inefficiency of iron packaging result in low detection sensitivity in terms of numbers of cells able to be detected. This weak cell labeling may restrict the types of clinical evaluations that MRI can potentially be used for, because a lot of labeled cells are required for detection. Labeling with weak magnetic particles will not be useful clinically for detecting cells that migrate away from cell transplants, it will not be useful clinically for tracking infiltration of immune cells for early diagnosis of disease, and it will not be useful for research in discovering new migration pathways or rare cell types. Conversely, we have demonstrated here how highly magnetic PLGA encapsulated magnetite MPs and NPs can label cells with 10 to 50-fold higher magnetite content without affecting cellular phenotype. We demonstrated here how this high magnetic labeling affords the detection of 10 cells or less by MRI, and would likely afford detection of individual cells in an appropriate model (19–21). Thus the detection sensitivity afforded by the use of PLGA encapsulated magnetite MPs and NPs as the labeling agent can potentially enhance clinical management and provide unique capabilities for disease detection and research endeavors.

The second key determination will be the likelihood of these particles to achieve FDA approval. The particles reported in this paper are composed of only two entities – iron oxide nanocrystals and PLGA. These two chemicals are mixed together into particles ranging from ~100 nm to 920 nm. Independently, each of these two chemicals is present in numerous FDA approved drugs. Iron oxide is the core component of ferumoxytol and ferumoxides, and is also FDA approved for use in cosmetics. Several PLGA based drug formulations are FDA approved and in clinical use including Decapeptyl SR, Nutropi Depot, Risperdal Consta, Sandostati LAR, Vivitrol and Trelstar. Thus, while the exact PLGA/magnetite construct needs to be tested for FDA approval, the simplicity of its makeup and the prior FDA approval of each of its two constituents, provides a more facile way forward to approval than if the particle were formed from components not already FDA approved. Indeed, with respect to FDA approval, there is little difference between the combination of iron oxide and PLGA into a new nanocomplex, and the combination of ferumoxytol, heparin and protamine – none of which are FDA approved for magnetic cell labeling – into one new nanocomplex, as proposed for HPF (17).

In conclusion, biodegradable and highly magnetic particles were fabricated with an FDA-approved polymer (PLGA) and were evaluated in multiple stem and immune cell assays, including viability, stem cell differentiation, and immune cell cytokine release. Additionally, particles were assessed for MRI-based cell tracking, using a transplantation paradigm and an innovative neural progenitor cell migration paradigm in which 10 cells were robustly

detected by MRI. Not only did neural and mesenchymal stem cells remain viable following labeling with magnetic particles, they also retained their ability to differentiate into multiple lineages in culture with similar proportions of differentiated cells. Furthermore, magnetically labeled immune cells were able to secrete appropriate levels of cytokines following stimulation. Taken together, these results demonstrate the potential of these particles for use as clinically viable contrast agents for MRI-based cell tracking and have the efficacy to enable highly sensitive cell detection by MRI in humans.

Conclusion

In this work, we described the preparation and pre-clinical evaluation of PLGA encapsulated magnetic particles for MRI-based cell tracking. Highly magnetic nano- (~100 nm) and microparticles (~1–2 μm) were fabricated using single oil-in-water emulsion technology and highly characterized. Magnetic particles were able to rapidly label cells in culture, within 3 hours delivering high amounts of iron to cells (50–150 pg Fe/cell). Notably, this was accomplished without the requirement of a transfection agent, and with no effect on cell viability. In rigorous experiments, the capability of magnetically labeled mesenchymal or neural stem cells to differentiate down multiple lineages, or for magnetically labeled immune cells to release cytokines following stimulation, was uncompromised. Testing their use for MRI, as few as 10 magnetically labeled cells, transplanted into the brains of rats, could be detected. To further test their use for MRI-based cell tracking, these particles enabled the *in vivo* monitoring of endogenous neural progenitor cell migration in rat brains over 2 weeks, achieving higher contrast to noise ratio than inert micron-sized iron oxide particles (MPIOs). The robust MRI properties and benign safety profile of these particles make them promising candidates for clinical translation for MRI-based cell tracking and would potentially enable highly sensitive detection of transplanted cells in humans.

Supplementary Material

Refer to Web version on PubMed Central for supplementary material.

Acknowledgments

We acknowledge Shauna Quinn for performing animal surgeries. Financial support from NIH grants P30 NS052519 and DP2 OD004362 is acknowledged.

References

1. Bulte JW. In vivo MRI cell tracking: clinical studies. AJR Am J Roentgenol. 2009; 193(2):314–325. [PubMed: 19620426]
2. Shapiro EM, Skrtic S, Koretsky AP. Sizing it up: cellular MRI using micron-sized iron oxide particles. Magn Reson Med. 2005; 53(2):329–338. [PubMed: 15678543]
3. Shapiro EM, Skrtic S, Sharer K, Hill JM, Dunbar CE, Koretsky AP. MRI detection of single particles for cellular imaging. Proc Natl Acad Sci U S A. 2004; 101(30):10901–10906. [PubMed: 15256592]
4. Bulte JW, Douglas T, Witwer B, Zhang SC, Strable E, Lewis BK, Zywicke H, Miller B, van Gelderen P, Moskowitz BM, Duncan ID, Frank JA. Magnetodendrimers allow endosomal magnetic labeling and in vivo tracking of stem cells. Nat Biotechnol. 2001; 19(12):1141–1147. [PubMed: 11731783]

5. Hill JM, Dick AJ, Raman VK, Thompson RB, Yu ZX, Hinds KA, Pessanha BS, Guttman MA, Varney TR, Martin BJ, Dunbar CE, McVeigh ER, Lederman RJ. Serial cardiac magnetic resonance imaging of injected mesenchymal stem cells. Circulation. 2003; 108(8):1009–1014. [PubMed: 12912822]
6. Kircher MF, Allport JR, Graves EE, Love V, Josephson L, Lichtman AH, Weissleder R. In vivo high resolution three-dimensional imaging of antigen-specific cytotoxic T-lymphocyte trafficking to tumors. Cancer Res. 2003; 63(20):6838–6846. [PubMed: 14583481]
7. Artemov D, Bhujwalla ZM, Bulte JW. Magnetic resonance imaging of cell surface receptors using targeted contrast agents. Curr Pharm Biotechnol. 2004; 5(6):485–494. [PubMed: 15579038]
8. Benderbous S, Corot C, Jacobs P, Bonnemain B. Superparamagnetic agents: physicochemical characteristics and preclinical imaging evaluation. Acad Radiol. 1996; 3 (Suppl 2):S292–S294. [PubMed: 8796583]
9. Raynal I, Prigent P, Peyramaure S, Najid A, Rebuzzi C, Corot C. Macrophage endocytosis of superparamagnetic iron oxide nanoparticles: mechanisms and comparison of ferumoxides and ferumoxtran-10. Invest Radiol. 2004; 39(1):56–63. [PubMed: 14701989]
10. Saleh A, Schroeter M, Ringelstein A, Hartung HP, Siebler M, Modder U, Jander S. Iron oxide particle-enhanced MRI suggests variability of brain inflammation at early stages after ischemic stroke. Stroke. 2007; 38(10):2733–2737. [PubMed: 17717318]
11. Levy M, Luciani N, Alloyeau D, Elgrabli D, Deveaux V, Pechoux C, Chat S, Wang G, Vats N, Gendron F, Factor C, Lotersztajn S, Luciani A, Wilhelm C, Gazeau F. Long term in vivo biotransformation of iron oxide nanoparticles. Biomaterials. 2011; 32(16):3988–3999. [PubMed: 21392823]
12. Arbab AS, Bashaw LA, Miller BR, Jordan EK, Bulte JW, Frank JA. Intracytoplasmic tagging of cells with ferumoxides and transfection agent for cellular magnetic resonance imaging after cell transplantation: methods and techniques. Transplantation. 2003; 76(7):1123–1130. [PubMed: 14557764]
13. Kalish H, Arbab AS, Miller BR, Lewis BK, Zywicke HA, Bulte JW, Bryant LH Jr, Frank JA. Combination of transfection agents and magnetic resonance contrast agents for cellular imaging: relationship between relaxivities, electrostatic forces, and chemical composition. Magn Reson Med. 2003; 50(2):275–282. [PubMed: 12876703]
14. Frank JA, Miller BR, Arbab AS, Zywicke HA, Jordan EK, Lewis BK, Bryant LH Jr, Bulte JW. Clinically applicable labeling of mammalian and stem cells by combining superparamagnetic iron oxides and transfection agents. Radiology. 2003; 228(2):480–487. [PubMed: 12819345]
15. Arbab AS, Yocum GT, Kalish H, Jordan EK, Anderson SA, Khakoo AY, Read EJ, Frank JA. Efficient magnetic cell labeling with protamine sulfate complexed to ferumoxides for cellular MRI. Blood. 2004; 104(4):1217–1223. [PubMed: 15100158]
16. Janic B, Rad AM, Jordan EK, Iskander AS, Ali MM, Varma NR, Frank JA, Arbab AS. Optimization and validation of FePro cell labeling method. PLoS One. 2009; 4(6):e5873. [PubMed: 19517015]
17. Thu MS, Bryant LH, Coppola T, Jordan EK, Budde MD, Lewis BK, Chaudhry A, Ren J, Varma NR, Arbab AS, Frank JA. Self-assembling nanocomplexes by combining ferumoxytol, heparin and protamine for cell tracking by magnetic resonance imaging. Nat Med. 2012; 18(3):463–467. [PubMed: 22366951]
18. Hinds KA, Hill JM, Shapiro EM, Laukkanen MO, Silva AC, Combs CA, Varney TR, Balaban RS, Koretsky AP, Dunbar CE. Highly efficient endosomal labeling of progenitor and stem cells with large magnetic particles allows magnetic resonance imaging of single cells. Blood. 2003; 102(3): 867–872. [PubMed: 12676779]
19. Shapiro EM, Sharer K, Skrtic S, Koretsky AP. In vivo detection of single cells by MRI. Magn Reson Med. 2006; 55(2):242–249. [PubMed: 16416426]
20. Heyn C, Ronald JA, Mackenzie LT, MacDonald IC, Chambers AF, Rutt BK, Foster PJ. In vivo magnetic resonance imaging of single cells in mouse brain with optical validation. Magn Reson Med. 2006; 55(1):23–29. [PubMed: 16342157]

21. Wu YL, Ye Q, Foley LM, Hitchens TK, Sato K, Williams JB, Ho C. In situ labeling of immune cells with iron oxide particles: an approach to detect organ rejection by cellular MRI. Proc Natl Acad Sci U S A. 2006; 103(6):1852–1857. [PubMed: 16443687]
22. Wischke C, Schwendeman SP. Principles of encapsulating hydrophobic drugs in PLA/PLGA microparticles. Int J Pharm. 2008; 364(2):298–327. [PubMed: 18621492]
23. Lo CT, Van Tassel PR, Saltzman WM. Poly(lactide-co-glycolide) nanoparticle assembly for highly efficient delivery of potent therapeutic agents from medical devices. Biomaterials. 2010; 31(13): 3631–3642. [PubMed: 20149428]
24. Kumari A, Yadav SK, Yadav SC. Biodegradable polymeric nanoparticles based drug delivery systems. Colloids Surf B Biointerfaces. 2010; 75(1):1–18. [PubMed: 19782542]
25. Shive MS, Anderson JM. Biodegradation and biocompatibility of PLA and PLGA microspheres. Adv Drug Deliv Rev. 1997; 28(1):5–24. [PubMed: 10837562]
26. Nkansah MK, Thakral D, Shapiro EM. Magnetic poly(lactide-co-glycolide) and cellulose particles for MRI-based cell tracking. Magn Reson Med. 2011; 65(6):1776–1785. [PubMed: 21404328]
27. Bennewitz MF, Tang KS, Markakis EA, Shapiro EM. Specific chemotaxis of magnetically labeled mesenchymal stem cells: implications for MRI of glioma. Mol Imaging Biol. 2012; 14(6):676–687. [PubMed: 22418788]
28. Weischenfeldt J, Porse B. Bone Marrow-Derived Macrophages (BMM): Isolation and Applications. CSH Protoc. 2008; 2008 db.
29. Briley-Saebo K, Hustvedt SO, Haldorsen A, Bjornerud A. Long-term imaging effects in rat liver after a single injection of an iron oxide nanoparticle based MR contrast agent. J Magn Reson Imaging. 2004; 20(4):622–631. [PubMed: 15390223]
30. Briley-Saebo K, Bjornerud A, Grant D, Ahlstrom H, Berg T, Kindberg GM. Hepatic cellular distribution and degradation of iron oxide nanoparticles following single intravenous injection in rats: implications for magnetic resonance imaging. Cell Tissue Res. 2004; 316(3):315–323. [PubMed: 15103550]
31. Briley-Saebo KC, Johansson LO, Hustvedt SO, Haldorsen AG, Bjornerud A, Fayad ZA, Ahlstrom HK. Clearance of iron oxide particles in rat liver: effect of hydrated particle size and coating material on liver metabolism. Invest Radiol. 2006; 41(7):560–571. [PubMed: 16772849]
32. Shapiro EM, Gonzalez-Perez O, Garcia-Verdugo JM, Alvarez-Buylla A, Koretsky AP. Magnetic resonance imaging of the migration of neuronal precursors generated in the adult rodent brain. Neuroimage. 2006; 32(3):1150–1157. [PubMed: 16814567]
33. Granot D, Scheinost D, Markakis EA, Papademetris X, Shapiro EM. Serial monitoring of endogenous neuroblast migration by cellular MRI. Neuroimage. 2011; 57(3):817–824. [PubMed: 21571076]
34. Sun S, Zeng H, Robinson DB, Raoux S, Rice PM, Wang SX, Li G. Monodisperse MFe2O4 (M = Fe, Co, Mn) nanoparticles. J Am Chem Soc. 2004; 126(1):273–279. [PubMed: 14709092]
35. Reich G. Ultrasound-induced degradation of PLA and PLGA during microsphere processing: influence of formulation variables. Eur J Pharm Biopharm. 1998; 45(2):165–171. [PubMed: 9704913]
36. Bennewitz MF, Lobo TL, Nkansah MK, Ulas G, Brudvig GW, Shapiro EM. Biocompatible and pH-Sensitive PLGA Encapsulated MnO Nanocrystals for Molecular and Cellular MRI. Acs Nano. 2011; 5(5):3438–3446. [PubMed: 21495676]
37. Bowen CV, Zhang XW, Saab G, Gareau PJ, Rutt BK. Application of the static dephasing regime theory to superparamagnetic iron-oxide loaded cells. Magnetic Resonance in Medicine. 2002; 48(1):52–61. [PubMed: 12111931]
38. Hirsjarvi S, Peltonen L, Hirvonen J. Effect of sugars, surfactant, and tangential flow filtration on the freeze-drying of poly(lactic acid) nanoparticles. AAPS PharmSciTech. 2009; 10(2):488–494. [PubMed: 19381823]
39. Hirsjarvi S, Peltonen L, Kainu L, Hirvonen J. Freeze-drying of low molecular weight poly(L-lactic acid) nanoparticles: effect of cryo- and lyoprotectants. J Nanosci Nanotechnol. 2006; 6(9–10): 3110–3117. [PubMed: 17048525]

40. Schachner M, Kim SK, Zehnle R. Developmental expression in central and peripheral nervous system of oligodendrocyte cell surface antigens (O antigens) recognized by monoclonal antibodies. Dev Biol. 1981; 83(2):328–338. [PubMed: 6786943]
41. Palfreyman JW, Thomas DG, Ratcliffe JG, Graham DI. Glial fibrillary acidic protein (GFAP): purification from human fibrillary astrocytoma, development and validation of a radioimmunoassay for GFAP-like immunoactivity. J Neurol Sci. 1979; 41(1):101–113. [PubMed: 438840]
42. Moody SA, Quigg MS, Frankfurter A. Development of the peripheral trigeminal system in the chick revealed by an isotype-specific anti-beta-tubulin monoclonal antibody. J Comp Neurol. 1989; 279(4):567–580. [PubMed: 2918088]
43. Shapiro EM, Medford-Davis LN, Fahmy TM, Dunbar CE, Koretsky AP. Antibody-mediated cell labeling of peripheral T cells with micron-sized iron oxide particles (MPIOs) allows single cell detection by MRI. Contrast Media Mol Imaging. 2007; 2(3):147–153. [PubMed: 17541955]
44. Dobrovolskaia MA, McNeil SE. Immunological properties of engineered nanomaterials. Nat Nanotechnol. 2007; 2(8):469–478. [PubMed: 18654343]
45. Duyn JH. Study of brain anatomy with high-field MRI: recent progress. Magn Reson Imaging. 2010; 28(8):1210–1215. [PubMed: 20392587]
46. Doetsch F, Caille I, Lim DA, Garcia-Verdugo JM, Alvarez-Buylla A. Subventricular zone astrocytes are neural stem cells in the adult mammalian brain. Cell. 1999; 97(6):703–716. [PubMed: 10380923]
47. Heyn C, Bowen CV, Rutt BK, Foster PJ. Detection threshold of single SPIO-labeled cells with FIESTA. Magn Reson Med. 2005; 53(2):312–320. [PubMed: 15678551]
48. Nohroudi K, Arnhold S, Berhorn T, Addicks K, Hoehn M, Himmelreich U. In vivo MRI stem cell tracking requires balancing of detection limit and cell viability. Cell Transplant. 2009; 19(4):431–441. [PubMed: 20149297]
49. Crabbe A, Vandeputte C, Dresselaers T, Sacido AA, Verdugo JM, Eyckmans J, Luyten FP, Van LK, Verfaillie CM, Himmelreich U. Effects of MRI Contrast Agents on the Stem cell Phenotype. Cell Transplant. 2010; 19(8):919–936. [PubMed: 20350351]
50. Montet-Abou K, Montet X, Weissleder R, Josephson L. Cell internalization of magnetic nanoparticles using transfection agents. Mol Imaging. 2007; 6(1):1–9. [PubMed: 17311760]
51. Walczak P, Ruiz-Cabello J, Kedziorek DA, Gilad AA, Lin S, Barnett B, Qin L, Levitsky H, Bulte JW. Magnetoelectroporation: improved labeling of neural stem cells and leukocytes for cellular magnetic resonance imaging using a single FDA-approved agent. Nanomedicine. 2006; 2(2):89–94. [PubMed: 17292120]
52. Qiu B, Xie D, Walczak P, Li X, Ruiz-Cabello J, Minoshima S, Bulte JW, Yang X. Magnetosonoporation: instant magnetic labeling of stem cells. Magn Reson Med. 2010; 63(6): 1437–1441. [PubMed: 20512844]
53. Bulte JW, Kraitchman DL. Iron oxide MR contrast agents for molecular and cellular imaging. NMR Biomed. 2004; 17(7):484–499. [PubMed: 15526347]
54. Slotkin JR, Cahill KS, Tharin SA, Shapiro EM. Cellular magnetic resonance imaging: nanometer and micrometer size particles for noninvasive cell localization. Neurotherapeutics. 2007; 4(3):428–433. [PubMed: 17599708]
55. Walczak P, Kedziorek DA, Gilad AA, Barnett BP, Bulte JW. Applicability and limitations of MR tracking of neural stem cells with asymmetric cell division and rapid turnover: the case of the shiverer dysmyelinated mouse brain. Magn Reson Med. 2007; 58(2):261–269. [PubMed: 17654572]
56. Tanimoto A, Oshio K, Suematsu M, Pouliquen D, Stark DD. Relaxation effects of clustered particles. J Magn Reson Imaging. 2001; 14(1):72–77. [PubMed: 11436217]

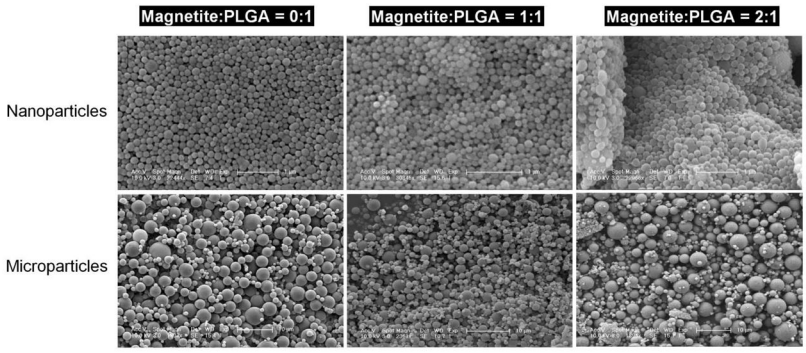

Figure 1.

Scanning electron micrographs of magnetic PLGA particles made with 2 concentrations of magnetite — first column is 0:1 magnetite/PLGA, second column is 1:1 magnetite/PLGA and third column is 2:1 magnetite/PLGA. Top row is nanoparticles and bottom row is microparticles. Note the regular, spherical appearance of all fabricated particles. Scale bar is 1 μm for NPs and 10 μm for MPs.

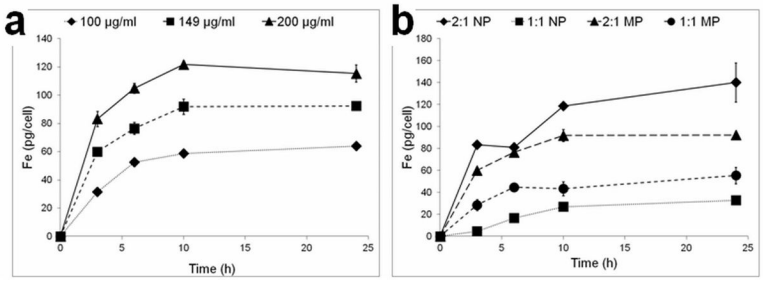

Figure 2.

Temporal labeling dynamics for a) 2:1 MP using three doses in Table 2 and b) for all four particles using only Dose 2. Data are means +/− SEM. In a) statistical insignificance is reached after 6 hours labeling for the two lowest doses, while it is reached for the high dose ($p<0.05$) after 10 hours. In b) statistical significance in intracellular iron content was measured ($p<0.01$) between MP and NP formulations at all time points.

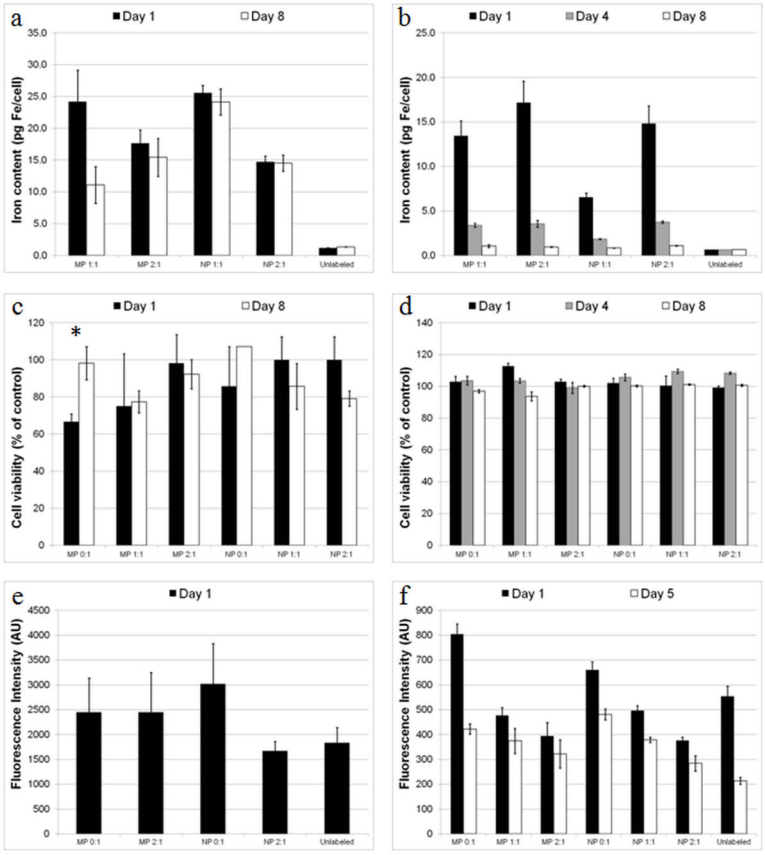

Figure 3.

Cellular iron content and physiology for labeled and unlabeled cells. Cellular iron content for a) slow dividing MSCs and b) fast dividing STOs as a function of time and particle type. Cell viability for c) slow dividing MSCs (* = $p < 0.05$) and d) fast dividing STOs as a function of time and particle type. ROS production for e) macrophages and f) STOs as a function of time and particle type. Data are means +/− SEM.

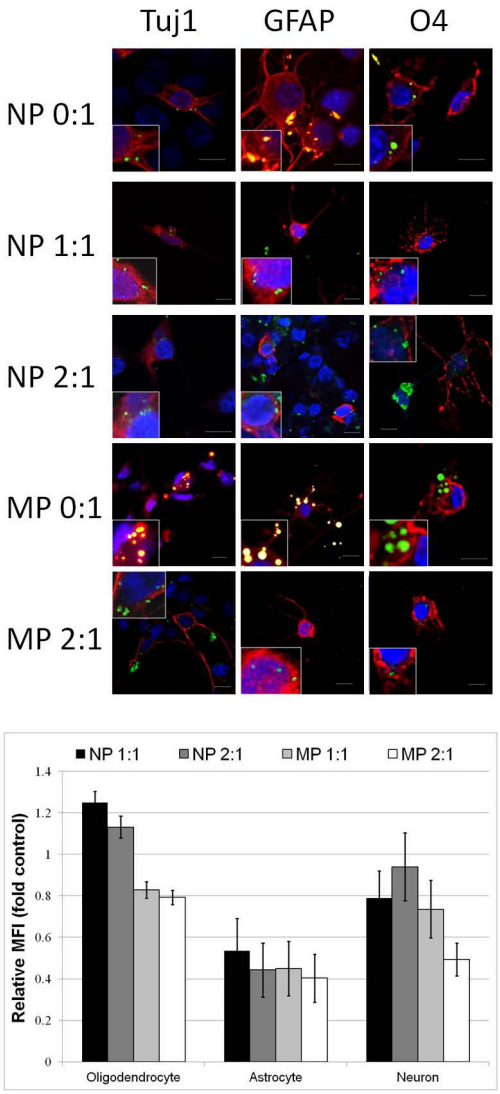

Figure 4.

a) Confocal fluorescence microscopy analysis of neural stem cell differentiation. Row and column headers indicate particle type and antigen stained for. All primary antibodies were labeled with secondaries that fluoresce red showing Tuj1+ neurons, GFAP+ astrocytes, or O4+ oligodendrocytes. Nuclear DNA is labeled with 4′,6-diamidino-2-phenylindole (DAPI) shown in blue, while green fluorescence is that of coumarin-6 incorporated in particles. For non-magnetic particles, bleeding from the green channel to the red channel was observed as orange overlap, possibly due to very high levels of coumarin-6 incorporation. Insets show digital expansions of cells highlighting intracellular presence of particles. Scale bar is 10 microns. b) Quantification of proportion of differentiated cell type relative to unlabeled cells. Data are means +/− SEM.

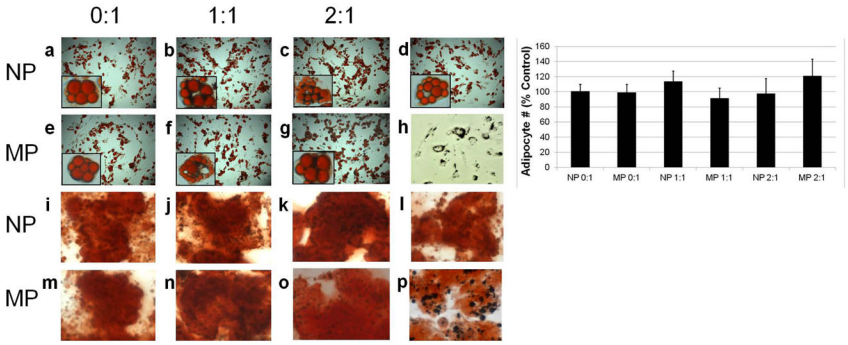

Figure 5.

Light microscopy of mesenchymal stem cell labeling and differentiation. Top two rows are adipogenic differentiation (Oil red O staining). Bottom two rows are osteogenic differentiation (Alizarin red staining). Row and column headers indicate particle formulation. Panels d and l) are differentiation of unlabeled cells. Panel h) is cells labeled with 1:1 MP prior to differentiation. Panel p) is a digital zoom of panel o) showing the presence of particles in the cells. Insets in a–g) are optical zoomed images of individual adipocytes containing particles, or for panel d), no particles. Chart compares proportion of labeled cells that differentiated into adipocytes to unlabeled cells that differentiated into adipocytes. Data are means +/− s.d.

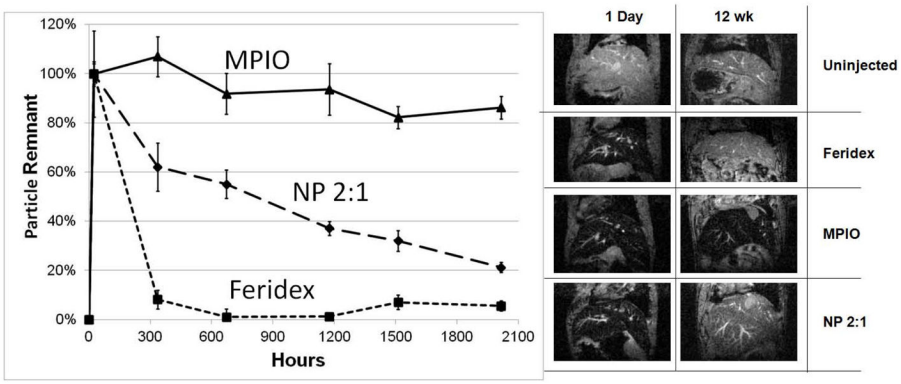

Figure 6.

In vivo biodegradation over 12 weeks following intravenous injection of Feridex, inert MPIOs and NP 2:1. Data are mean +/− SEM. MRI of mice livers are at TE = 6 ms for mice injected as indicated, both at 1 day and 12 weeks following injection.

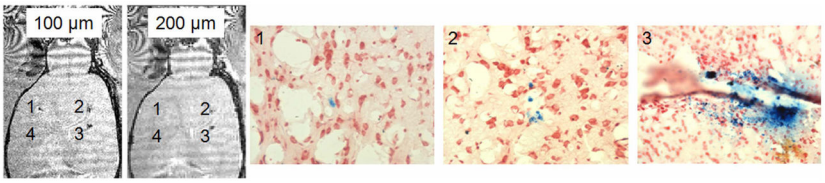

Figure 7.

In vivo MRI of transplanted stem cells. 3D MRI acquired at either 100 or 200 microns with 1) 10 cells, 2) 100 cells, 3) 1000 cells or 4) 1000 unlabeled cells. Accompanying Prussian Blue histology from appropriate locations (1, 2 or 3) showing general number of cells detected at each location.

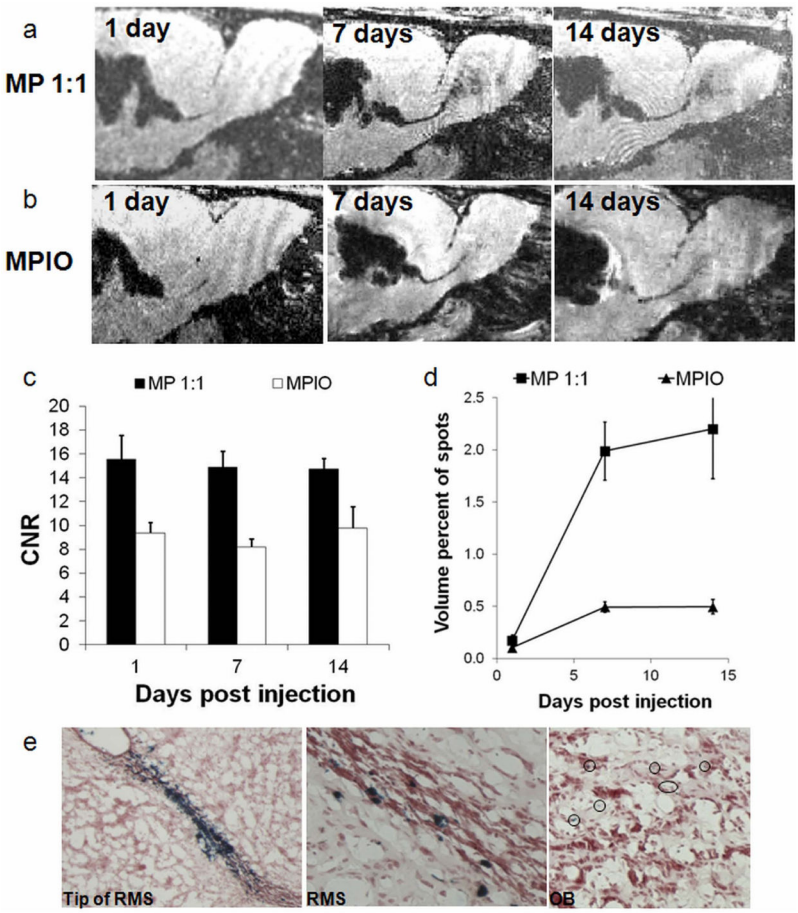

Figure 8.

In vivo MRI of endogenous neuroblasts migration. MRI montage of same animal at level of SVZ – RMS – OB injected with a) MP 1:1 or b) inert MPIOs. Days of MRI are given in panels. c) CNR measurement of dark contrast within RMS. d) Volume of dark contrast in the OB. e) Prussian blue staining for iron in SVZ, RMS, and OB showing presence of iron specifically and throughout the migratory pathway. Data in panels c and d are mean +/− SEM.

Table 1

Physical and MRI characteristics of the different magnetic PLGA particles made for this study, showing particle size and iron oxide content. Particle size values are mean +/− s.d. n> 50 particles.

Particle characteristics	nanoparticles			microparticles		
Magnetite:PLGA	0:1	1:1	2:1	0:1	1:1	2:1
Particle size, nm	105±37	95±34	105±62	2100±1100	920±510	920±790
Magnetite content, wt%	0	56.7	83.7	0	58.2	66.1
r_2, $s^{-1}mM^{-1}$ iron	-	196	28.5	-	44.7	38.7
r_2, $s^{-1}mM^{-1}$ particle	-	8.91×10^8	3.95×10^8	-	1.937×10^{11}	2.11×10^{11}
r_2*, $s^{-1}mM^{-1}$ iron	-	659.1	243	-	384.1	614.1
r_2*, $s^{-1}mM^{-1}$ particle	-	2.99×10^9	3.37×10^9	-	1.65×10^{12}	3.35×10^{12}

Magn Reson Med. Author manuscript; available in PMC 2015 February 21.

Table 2

Particle doses used for magnetic cell labeling. All three doses were tested for magnetic cell labeling in fibroblasts. Dose 2 was used for cell labeling of neural and mesenchymal stem cells, and immune cells.

	1:1 NP	**2:1 NP**	**1:1 MP**	**2:1 MP**
Dose 1 (μg/mL)	100	150	100	100
# particles	71.4×10^9	69.9×10^9	8.8×10^6	7.8×10^6
Iron concentration (mM)	0.73	1.06	0.75	0.77
Dose 2 (μg/mL)	137	210	133	149
# particles	97.8×10^9	97.8×10^9	11.7×10^6	11.7×10^6
Iron concentration (mM)	1.00	1.48	1.00	1.15
Dose 3 (μg/mL)	200	250	200	200
# particles	142.8×10^9	116.4×10^9	17.6×10^6	15.6×10^6
Iron concentration (mM)	1.46	1.76	1.50	1.54